Journal of The Electrochemical Society

The Electrochemical Society
Advancing solid state & electrochemical science & technology

OPEN ACCESS

Evaluating the Manufacturing Quality of Lithium Ion Pouch Batteries

To cite this article: Lingxi Kong *et al* 2022 *J. Electrochem. Soc.* **169** 040541

View the article online for updates and enhancements.



ECS Membership = Connection

ECS membership connects you to the electrochemical community:

- Facilitate your research and discovery through ECS meetings which convene scientists from around the world;
- Access professional support through your lifetime career:
- Open up mentorship opportunities across the stages of your career;
- Build relationships that nurture partnership, teamwork—and success!

Join ECS! Visit electrochem.org/join

This content was downloaded from IP address 88.255.99.35 on 27/07/2022 at 12:06

Journal of The Electrochemical Society, 2022 **169** 040541

Evaluating the Manufacturing Quality of Lithium Ion Pouch Batteries

Lingxi Kong,[1,z] Ryan Aalund,[1] Mohammad Alipour,[2] Stanislav I. Stoliarov,[3] and Michael Pecht[1]

[1]*Center for Advanced Life Cycle Engineering (CALCE), University of Maryland, College Park, Maryland 20742, United States of America*
[2]*Koç University Tüpraş Energy Center, Rumelifeneri Yolu, Istanbul, Turkey*
[3]*Department of Fire Protection Engineering, University of Maryland, College Park, Maryland 20742, United States of America*

Lithium-ion batteries must undergo a series of quality control tests before being approved for sale. In this study, quality control tests were carried out on two types of lithium-ion pouch batteries, here denoted as type A (with stacked electrode configuration) and type B (with a jelly-roll arrangement) to assess the effectiveness of the tests. Electrochemical tests, which included capacity and impedance measurements, found that both types of batteries met the specifications. However, computed tomography (CT) scan, disassembly, and material characterization revealed quality concerns in battery assembly and material composition. Results showed that, for an A cell, cathode extended past anode at the top and bottom of the roll, and a CT scan revealed inhomogeneities in the electrode near the corners. Similarly, analysis of a B cell revealed gaps in the winding structure and cathode material discrepancies. More specifically, the lithium nickel manganese cobalt oxide (NMC) material specified by the battery manufacturer turned out to be lithium cobalt oxide (LCO). The findings indicate that systematic quality control tests are needed to properly identify defects in batteries before they are used in products.
© 2022 The Author(s). Published on behalf of The Electrochemical Society by IOP Publishing Limited. This is an open access article distributed under the terms of the Creative Commons Attribution 4.0 License (CC BY, http://creativecommons.org/licenses/by/4.0/), which permits unrestricted reuse of the work in any medium, provided the original work is properly cited. [DOI: 10.1149/1945-7111/ac6539]

Manuscript submitted January 5, 2022; revised manuscript received March 21, 2022. Published April 19, 2022.

The use of lithium-ion batteries (LIBs) increases across applications of automobiles, stationary energy storage, consumer electronics, medical devices, aviation, and automated infrastructure,[1–6] assuring the battery quality becomes increasingly essential. Original equipment manufacturers (OEMs) have responsibility for customer safety since they integrate various components into the final product ready for consumers. As a key part of the final device, sufficient quality tests on the LIBs can lower the risk of undesirable customer-facing outcomes, such as draining of battery, unexpected shutdown,[7] and especially a thermal runaway which may result in fire. LIB manufacturers use several standards to assess the safety of the design, including IEC 62133, UL 1642, and UN 38.3. These standards consist of a series of tests executed on a specified number of samples (five samples required in most tests) for preventing instant failure. However, standards-based testing fails to assess battery quality-related issues. These issues can pose a potential hazard. Getting certification for battery standards is a one-time event on a defined number of samples. Testing does not account for manufacturing variance beyond the initial sample. Manufacturing variance can lead to nonuniform electrode coating, separator pinholes, and electrode misalignment, which may negatively impact performance or manifest as a safety risk.

Quality control is a set of tools and processes used to assure that a product adheres to the specifications throughout the manufacturing process. Both the battery manufacturers and the OEMs of battery powered devices should apply the concept of quality control to the entire manufacturing process. For the battery manufacturers, the quality control covers steps from the raw material collection to the fabrication of components, including the electrode, separator, electrolyte, current collector, and the battery case/can and lid or pouch. Component-level quality control can screen out defective components before assembly, decrease the scrap rate, and reduce the waste cost from defective products.[8,9] Some of the quality control steps are embedded within the manufacturing process, such as the high potential (Hi-pot) test conducted during the separator manufacturing,[10] contamination level control during electrolyte solution manufacturing,[11] and the quality control during electrode manufacturing.[12,13] However, for the assembled batteries, there is only limited electrochemical performance-based quality control step, including impedance and capacity measurements.[12] Battery manufacturers conduct electrochemical tests as the final screening step before delivering their product. But electrochemical test alone is not sufficient to capture all the potential failure precursors made during battery manufacturing. The absence of the above-mentioned quality control steps, on both the battery manufacturer's and OEM's sides, could lead to potential issues that defective batteries be implemented in the final product. These defects could be introduced due to manufacturing and transportation issues, variances within the manufacturing and transportation process, or incorrect design.

Defects originating from the manufacturing process will have varying effects on the battery's safety and performance. Safety-related defects include compromised separator integrity, which may lead to a short circuit and thermal runaway.[14,15] Electrode overhang leads to dendrite growth and eventual short-circuit.[16] The failure rate of lithium-ion batteries is estimated to be 0.025 ppm,[17] 0.1 ppm,[17] or 1 ppm.[18] Although not all defects will develop into a failure, defects can hinder the performance of lithium-ion batteries. Performance-related defects include agglomerates, pinholes, metal particle contaminants, and non-uniform coatings, these defects can lead to substandard capacity,[19] increased impedance,[20] higher degradation rate,[21] and reduced useful life.[22] These issues mainly originate from inconsistencies during electrode assembly, stacking/folding, electrolyte injection or wetting, and formation. Battery defects also can be amplified after formation.[23] The battery quality issues exist in various battery types, including the pouch batteries[23] and cylindrical batteries.[14,24] For large-scale battery applications such as electric vehicles, even a single battery level failure rate is as low as 0.1 ppm, the expected failure rate for electric vehicles can be 1 over 10,000 (100 ppm).[25] A quality control process is necessary to maintain consistency during the manufacturing process of LIBs.

The purpose of characterization tests is to guarantee that the battery and the battery embedded devices meet the designed performance per the specifications. Characterization tests on a LIB received from a battery manufacturer are critical to determining adherence to requirements, especially for the OEMs who have direct responsibility for the safety of end users. In addition, through conducting characterization tests on all received battery batches,

[z]E-mail: lkong@umd.edu

OEMs can build historical data of battery quality for evaluating the reliability capability of their battery suppliers and also make adjustment to their devices' operational range in time when there is a change in the battery properties. Such adjustments are necessary for ensuring sufficient safety margin to prevent potential abuse caused battery failure events.

Characterization tests can be classified as non-destructive and destructive. Nondestructive tests consist of dimension measurement; electrochemical tests including capacity tests,[26] open-circuit voltage (OCV) tests,[27] electrochemical voltage spectroscopy tests,[28] and internal impedance/resistance tests[9]; X-ray photography[29] and X-ray CT[30]; and neutron tomography.[31] In the electrochemical tests, mainly cell capacity, impedance/resistance, and OCV are measured to analyze the electrochemical performance of batteries. Cell capacity, OCV, and resistances provide valuable information on the maximum deliverable capacity under a given load, thermodynamic properties, and cell dynamics, respectively.[32] Because the electrochemical-based method does not change the original state of the cell, it can be adopted for inline quality control.[33] Despite being an expensive method requiring a longer measurement time, CT determines the battery's internal structure without disassembly.[34] Many researchers have deployed it to evaluate the battery cell internal deformation after aging,[35] mechanical stress,[36] failure,[37] and abuse tests.[38] As mentioned in the IEEE 1625 standard, "A vision system, such as X-ray check, shall be used to ensure electrode integrity at an appropriate point in the assembly process".[39] The CT scanning result for an intact or qualified battery can be regarded as the comparison baseline to check manufacturing quality. The neutron tomography gives valuable information on the macroscopic design inside the battery cell; however, it is not a common and practical method.[40]

Material degradation modes such as particle cracking and island formation,[41] graphite exfoliation,[42] lithium plating,[43] transition metal dissolution,[44] electrolyte degradation,[45] film formation on particles and electrode surfaces,[46] clogging of electrode pores,[47] closing of separator pores,[48] and binder decomposition[49] cannot be detected by non-destructive methods. Therefore, destructive methods are necessary for the detailed physicochemical analysis of battery cells. Destructive methods include disassembly and a corresponding visual check by microscopies such as optical microscopy, scanning electron microscopy (SEM), and transmission electron microscopy (TEM); chemical analysis methods sensitive to electrode surfaces such as energy dispersive X-ray spectroscopy (EDX), X-ray photoelectron spectroscopy (XPS), Fourier transform infrared spectroscopy (FTIR), and secondary ion mass spectroscopy (SIMS); chemical analysis methods for electrode bulk such as inductively coupled plasma optical emission spectrometry (ICP-OES), nuclear magnetic resonance (NMR), and X-ray diffraction (XRD); and finally electrolyte analysis such as NMR and gas chromatography (GC).[40] Disassembly and visual inspection are used to verify any suspicious spots found during the previous CT test. SEM is conducted on the electrodes, including the anode and cathode, to check their surface morphology and determine particle size distribution. It is usually combined with EDX to determine the chemical composition. XPS is surface-sensitive[50] and can be used to analyze chemical changes on the particle surface. Except for the helium and the hydrogen, XPS allows measuring the elemental composition and determining their oxidation states. FTIR is conducted to determine the organic components, including the electrolyte and the separator. In the ICP-OES technique, a sample from electrodes is being characterized after dissolving in an acid solution. Stiaszny et al.[51] used this technique to measure the concentration of transition metal at the anode. XRD can analyze the change in electrode structures and particle orientation. NMR and GC are the methods to analyze the soluble, insoluble, and gas products forming due to electrolyte decomposition.

Characterizing a lithium-ion battery should at least include an examination of the physical properties and electrochemical performance per the battery manufacturers' specifications. However, proper and thorough characterization determines not only the measured cell's OCV, specific capacity, specific energy, impedance, and physical dimensions, but also examines the material properties of the electrodes, separator, electrolyte, and assembly quality. Here the assembly quality related issues include debris, nonuniformity of electrode construction or assembly, and imperfections (e.g., unintentional folds or twists) in the assembly.

This paper demonstrates methods to assess the quality of lithium-ion pouch batteries (LiPBs) and in particular the limitation of electrochemical characterization tests which overlook potential failure precursors within a readily assembled LiPB. This paper also demonstrates the ability and importance of optical tests for capturing quality issues in battery assemblies and the use of material tests for ensuring the electrode material is consistent with the specification. To this end, methods including both destructive and non-destructive types are applied to both jelly-roll structured and stacking structured commercial LiPBs (five pouch cells from each type). All cells are subjected to electrochemical tests to characterize and analyze their manufacturing quality. In addition, one cell from each group undergoes a CT scan and disassembly to evaluate possible structural defects. Following the disassembly, SEM/EDX is used for the elemental analysis of the electrodes to confirm their types, and FTIR analysis is performed to determine the characteristics of the material of the separators. The experimental methods and the samples are introduced in experimental section. The characterization test results are presented in results section. The conclusions from these tests are provided in the last section.

Experimental

Method.—The selection of specific test methods is based on three principles. The first principle is about the capability; selected tests should reveal the battery's electrochemical performance, material, structure, and design. The second principle is about the availability of battery specification. For comparison, tests should cover the items mentioned in the battery specification. The third principle is practicality. In consideration of the mass production of the OEMs, the tests should take no more than a few weeks.

The conventional method focuses on the electrochemical performance of the battery and relies on the specification provided by the battery manufacturer. The methods developed in this study also involve structural and material characterization, especially the CT test which allows micro-meter level examination of the battery internal structure to reveal potential failure precursor. The following tests were conducted to characterize the battery quality and performance. Electrochemical properties were evaluated on all ten cells (five cells per type), including capacity measurement and 1 kHz impedance at 100% state of charge (SOC), and assessed in terms of the battery specification. The capacity measurement was conducted on the Arbin BT-I battery tester under the constant current discharge condition specified in the battery specification (0.2C and 3.0 V cut-off voltage at room condition). The impedance measurement was conducted on the Agilent LCR meter. Samples were manufactured in the same batch, and a CT scan was conducted to determine the design inside one of the five cells. A 3D digital model of the tested cell was generated after scanning from all directions with a resolution of 30 micrometers.

After the non-destructive characterization tests, the cycled battery was sent for CT scan investigation and, subsequently, disassembled. Before disassembly, cells from both groups were discharged to the lower cut-off voltage, which is regarded as 0% SOC. The cell disassembly process was conducted in the glovebox filled with ultrahigh purity argon gas. The cells were disassembled to the component level, where the outer case, anode, cathode, and separator were detached from each other. Samples with a size of around 1×1 cm^2 were cut from anode, cathode, and separator for the following analysis. SEM/EDX analysis of battery electrodes was conducted on the FEI Quanta environmental scanning electron microscope with advanced energy dispersive spectroscopy to characterize the

electrode surface morphology and chemical elements. The EDX electrode elemental analysis was conducted on various points and the area mapping. Some of the cut electrode samples were embedded in the epoxy resin matrix and ground to reveal the electrode cross-section. The ground samples were observed under the ZEISS Axiovert microscope. The electrode thickness was measured with the corresponding imaging software. Cross-sectioning analysis of the disassembled battery electrodes was conducted to identify particle distribution and the electrode's thickness. With the Agilent Cary 670 FTIR Spectrometer, FTIR analysis of the extracted battery separator was conducted to determine characteristics of the material of the separators after cleaning. The separator samples were also cut from the disassembled battery with a size of about 1×1 cm^2. The characterization results are reported in the next section.

Samples.—In this study, the jelly-roll and stacking structured pouch LIBs were studied. To fully understand their internal structure and design, their manufacturing process is reviewed as follows. Pouch-formed LIBs are manufactured through either a jelly-roll winding process or a stacking process. Figure 1a shows an expanded view of the winding process. For the jelly-roll winding process, the electrodes and separator are in a long ribbon form. The separator is sandwiched between the anode and the cathode. Winding the sandwiched layers up leads to a jelly-roll structure or a LIB cell core.[52]

The expanded view of a stacking structured pouch LIB is shown in Fig. 1b. Unlike the winding process, in the stacking method, the anode and cathode are cut into multiple pieces with an area slightly smaller than the outer size of the LIB. The next step is stacking these pieces of anode, cathode, and separator in the sequence of the anode, separator, cathode, separator, and anode again. By repeating this subassembly, electrodes can be added for a larger battery capacity. There are two ways of handling the separator. It can be cut into pieces and the electrodes are applied in the stacking process.[53,54] The other method does not cut the separator. However, zig-zag folds the separator to incorporate alternating layers of anode and cathode.[54]

This study tested 10 pouch cells from 2 vendors, including stacking and jelly-roll-structured pouch LIBs. The stacking-structured batteries from the first vendor were assigned the following code names: A-1, A-2, A-3, A-4, and A-5. The cells' dimensions were $88 \times 31 \times 8.7$ mm (max length/width/thickness). As indicated by the battery specification, the A-type cells had a nominal voltage of 3.7 V and a working voltage range of 3.0 to 4.2 V. The nominal capacity of the cells was 2.7 Ah (2700 mAh), which was determined under 0.2C with a 3.0 V cut-off voltage at room condition. The cell A manufacturer specification does not specify the cathode material type. Cathode material identification is also expected from the testing.

The B-type cells were the jelly-roll-structured pouch lithium-ion batteries named B-1, B-2, B-3, B-4, and B-5. Based on the battery specification, the cell's dimensions are $78 \times 31 \times 8.7$ mm (max length/width/thickness). The battery nominal voltage is 3.7 V with a working voltage range of 3.0 to 4.2 V. The nominal capacity of the cells was 3.0 Ah (3000 mAh) under conditions of 0.2C and 3.0 V cut-off voltage at room condition. The received battery specifications indicated the cathode was made of NMC. The samples and the corresponding tests are summarized in Table I.

Results

After receiving the samples, a quick visual inspection of the cells was performed, and no abnormalities were discovered. The characterization began with non-destructive analysis, which included electrochemical tests and a CT scan. After the non-destructive investigation was completed, samples from each vendor were selected for destructive analysis, including the SEM/EDX and FTIR. The destructive analysis also consisted of a visual inspection during the teardown step to look for nonconformities.

Characterization of electrochemical properties.—The battery specifications were checked to determine the electrochemical features of the battery. The first step was to evaluate the batteries' consistency by measuring the discharge capacity and the impedance. These two variables measure the battery performance since they are directly related to battery lifetime and power output. The electrochemical tests done at this stage are regarded as non-destructive tests because they do not significantly change the battery's internal structure.

Capacity measurement was conducted on all 10 cells. The cells were discharged to 3 V (0% SOC) before the cycling test in a semi-temperature controlled room with temperature of 25 ± 2 °C. After the initial discharge, all cells were charged (CCCV, constant

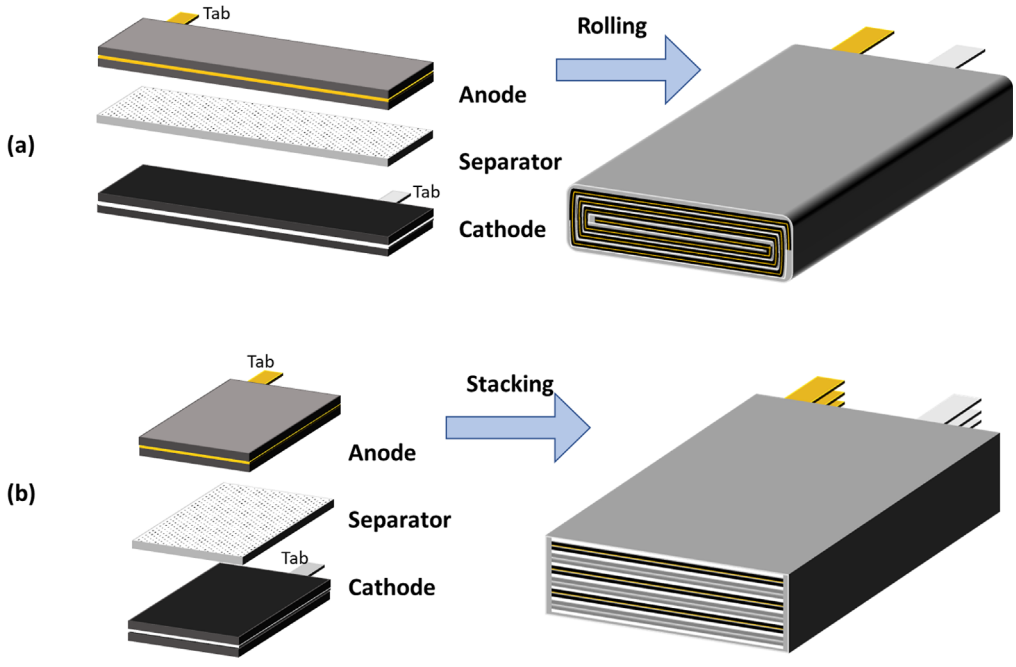


Figure 1. An expanded view and fully assembled lithium-ion cell using (a) the winding process and (b) the stacking method.

Table I. Summary of samples and corresponding tests.

Tests	A-type cells					B-type cells				
	A-1	A-2	A-3	A-4	A-5	B-1	B-2	B-3	B-4	B-5
capacity measurement	×	×	×	×	×	×	×	×	×	×
1 kHz impedance at 100% SOC	×	×	×	×	×	×	×	×	×	×
CT scan	×					×				
disassembly	×					×				
SEM/EDX	×					×				
electrode cross-section	×					×				
FTIR analysis	×					×				

current–constant voltage) and discharged (CC, constant current) for two cycles. The cell discharge capacity (@0.2C, 520 mA for A-type; 600 mA for B-type) from 2 cycles was recorded. The corresponding results are shown in Fig. 2. Except for cell A-1, which showed a discharge capacity of 2.67 Ah in the first cycle, all cells had a measured discharge capacity equal to or above the nominal capacity of 2.7 Ah. Cells A-2 to A-5 showed consistent discharge capacity in the range of 2.82 to 2.84 Ah with an average discharge capacity of 2.83 Ah. The B-type cells showed a capacity higher than the nominal capacity of 3.0 Ah. The average discharge capacity was 3.05 Ah. The ratio of the first-cycle discharge capacity to the second-cycle discharge capacity was higher than 99% for all 10 samples.

In addition to capacity tests, cell impedance measurements are also performed on all samples. The battery's impedance is a parameter related to its power output. Since the internal impedance was only provided for B-type samples ($\leqslant$30 mΩ) and the manufacturer's impedance measuring method was not specified, in this approach, the cells were fully charged to 100% SOC before impedance measurements at 1 kHz. Cells A-1 to A-5 showed impedance values in the range of 65 to 68 mΩ, consistent with each other. Similarly, cells B-1 to B-5 showed impedance values in the range of 68 to 71 mΩ. The samples showed no significant variance from the manufacturing process from both the electrochemical test and the impedance measurement.

Manufacturing defect examination assisted by CT scan.—After the electrochemical tests, cell A-1 was selected for the CT test. The 3D digital model generated for the tested cell allows checking from all aspects without disassembly. Figure 3a shows the CT images from cell A-1, including the top view, side view, front view, and the 3D model.

Based on the CT results, some unknown marks were found on cell A-1. As shown in Fig. 3b, there were four round-shaped marks on the four corners from the CT front view. Since the separator is made of organic material that does not significantly absorb X-rays, the marks are most likely related to the electrodes, which was later confirmed through the cell disassembly process (Fig. 3d). During the automatic manufacturing process, the assembly machine grabs and transfers the pieces of the electrodes at the four corners since the A-type cells have a stacking structure. At this stage, the force applied during manufacturing could cause the electrode coating layer deformation that left the marks seen from the CT images.

In addition to the uniformity of battery electrodes, electrode alignment is another aspect that needs to be checked. According to the IEEE 1725: Standard for rechargeable batteries for cellular telephones,[55] 'the manufacturer/supplier shall assure the accuracy of electrode placement. The manufacturer/supplier shall conduct 100% vision system inspection of the cell core to verify that the negative-to-positive electrode overlap is at least 0.1 mm on all sides, unless documented process analysis justifies a lesser minimum overlap'. Therefore, the CT scan was applied for checking the battery electrode alignment. In general, the anode will be longer than the cathode to guarantee coverage. However, as shown in Fig. 3c, the cathode is longer than the anode within the dashed white square indicating that the electrodes were not aligned properly. The misalignment increases the potential hazard of lithium dendrite growth. Since the cathode is longer than the anode, the edge of the anode is where the current density will be higher than the rest of the electrode surface. Brissot et al.[56] reported that the rate of dendrite growth on an anode is directly proportional to the local current density. Therefore, the increase of local current density and lithium-ion concentration caused by the electrode misalignment increases the risk of lithium deposition and dendrite growth.

To further evaluate the battery manufacturing quality and verify the marks found during the CT analysis, cell A-1 was disassembled after the CT. Before disassembly, cell A-1 was discharged to 3 V (0% SOC). By discharging the cell, the total amount of energy stored inside the battery was drained out, which can reduce the risk of short circuit during disassembly and reduce the activity of the electrode materials during and after disposal of the LIB.

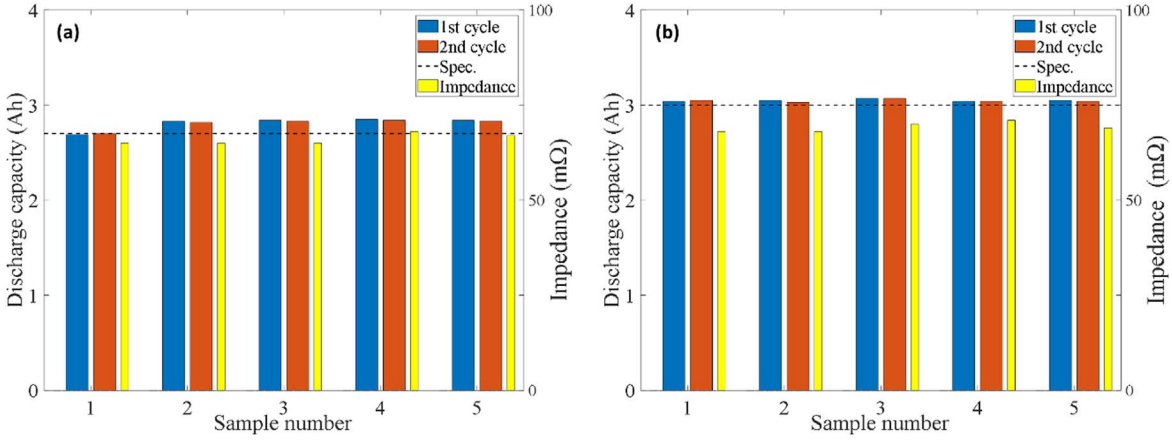


Figure 2. The discharge capacity in the first two cycles for (a) A-type (b) B-type cells. Dashed lines refer to the nominal capacity from the battery specifications.

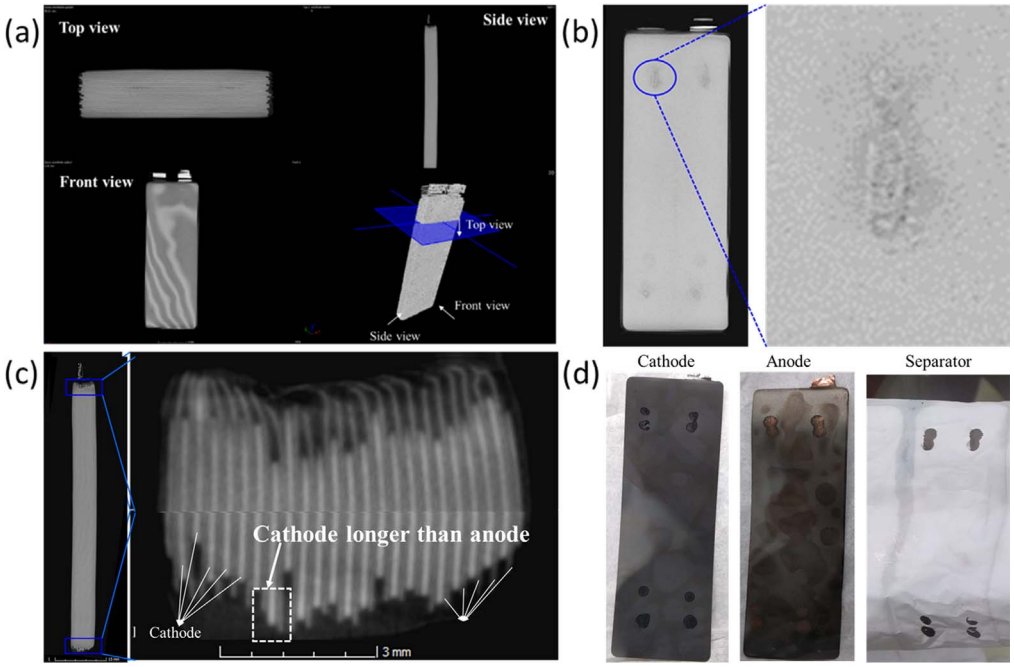


Figure 3. (a) CT images of cell A-1; (b) Unknown marks found in cell A-1; (c) Electrode alignment in cell A-1; (d) Electrodes from cell A-1: (from left to right) cathode, anode, and separator. Figures (a) to (c) are CT images and figure (d) is a regular photograph of disassembled parts.

Through the disassembly, it was found that cell A-1 had a stacking structure that had multiple layers of cathode and anode. There was also a current collector in each layer. The round marks on cathode and the anode (Fig. 3d) corresponded to the unknown marks observed in the CT. The observed marks on the electrodes can cause nonuniform degrees of lithiation inside the electrode material and consequently result in inhomogeneous degradation.[57] The separator was attached to the cathode/anode at the locations with marks (Fig. 3d), indicating that these spots experienced higher stress than the rest of the parts and may lead to cracks in the coating layer during long-term cycling. The black spots on the separator (Fig. 3d) were the electrode materials peeled off from the electrodes, indicating that the electrode materials at the four spots have a stronger adhesion to the separator than the rest. This could be caused by spots on the electrodes that experienced higher pressure during the battery assembly process.

Cell B-1 was also subjected to CT scan analysis. Figure 4a shows the CT images of cell B-1 including the top view, side view, front view, and the 3D model. Although no apparent electrode variance found on the electrode surface, abnormalities related with the electrode winding process were found from the CT scan of cell B-1. Figure 4b shows the existence of current collector folding and Fig. 4d shows a misshapen portion of the electrode. These abnormalities indicate that the manufacturing process was not well controlled.

Figure 4b showed the folded current collector in B-1 from the CT scan. The current collector is metallic and electrically conductive; therefore, a folded current collector will alter the local current distribution. Another potential concern is the extra friction between the folded current collector and the separator during longer-term operation. Since the battery is vacuum-sealed, the jelly-roll structure is under pressure from the battery's outer casing. Suppose the jelly-roll structure has a nonuniform thickness, such as the folded current collector. In that case, there could be a higher stress spot in this location.

An irregular anode in the battery core region, highlighted in Fig. 4d, indicates a lack of quality control during the electrode jelly-roll winding process. Similar to the above-mentioned concern about the current collectors, the concern here is also potential extra friction and a nonuniform current distribution, leading to localized current density increase and lithium plating on the anode.

Electrode alignment issues existed in the winding structure, which indicated the winding process was imprecise. The winding process is related to the alignment of the anode and cathode, which determines the current uniformity inside the battery. The electrode gap will cause nonuniform current distribution on the electrodes and may lead to localized lithiation. As illustrated in Fig. 4e, the presence of golden lines indicates inhomogeneous delithiation on the anode after being fully discharged.[58] Therefore, the electrode gap will cause nonuniform current distribution on the electrodes and lead to localized lithiation.

The electrode misalignment found in cell A-1 also existed in Cell B-1. As shown in Fig. 4c, the "thin" layers represent the anodes, and the "thick" layers represent the cathodes. The anode layers should be longer than the cathode layers to fully use the reversible lithium content and prevent the lithium dendrite formation on the electrode edge. The dashed squares show areas where the anode layers are not longer than the cathode layers. The misaligned electrodes indicates that there is a lack of precise control on the rolling process.

Electrode and separator material characterization after disassembly.—To check the composition of the electrodes, SEM/EDX analysis was performed on electrode samples from cells A-1 and B-1, and the elemental analysis results were as follows. The morphologies of the anode from cell A-1 and B-1 are illustrated by SEM images in Figs. 5a and 5c, respectively. Similarly, the anode elemental mapping is done using EDX analysis. The corresponding results are shown in Figs. 5b and 5d. The EDX mapping results revealed that the anodes are mainly composed of carbon element showing that graphite is used as anode material in both cells. In addition to the major elements, small amounts (<10%) of oxygen, sulfur, fluorine, phosphorus elements were also detected. The corresponding signals could be generated from the electrode binder, and residual electrolyte attached to the electrode. Table II lists the anode elemental composition of cells A-1 and B-1.

SEM micrographs for both cells' cathode and their corresponding EDX elemental mappings are shown in Fig. 6. The cathode elemental composition of cells A-1 and B-1 are listed in Table III.

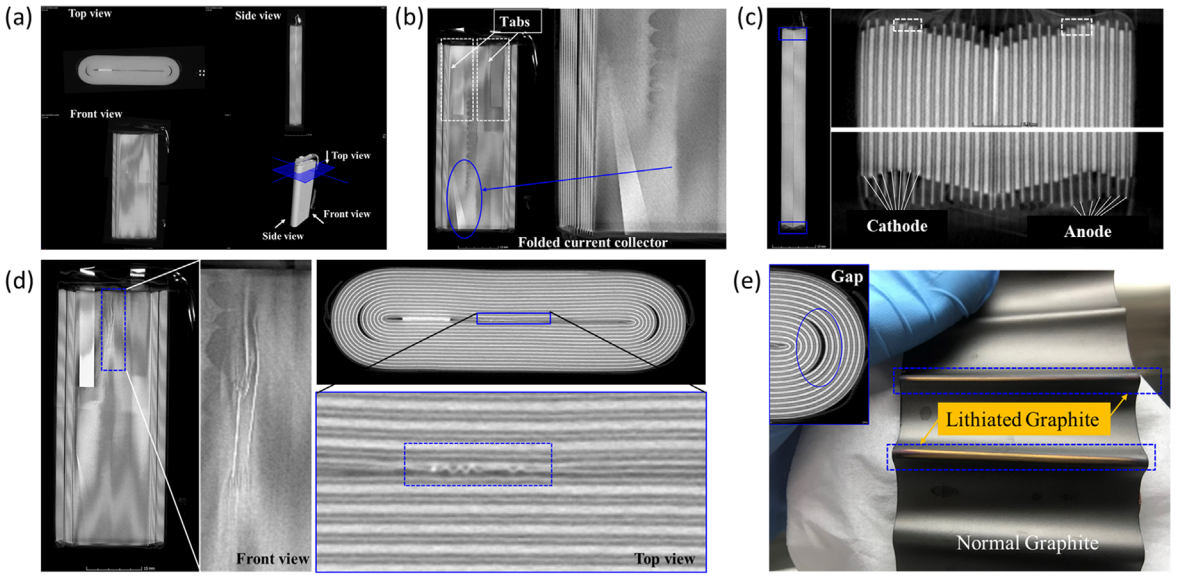


Figure 4. (a) CT images of cell B-1; (b) Folded current collector in cell B-1; (c) Electrode alignment in cell B-1; (d) A misshapen portion of anode in cell B-1: (left) front view and (right) top view; (e) The presence of the electrode gap and the gap-caused lithiated graphite in the discharged state found during disassembly of cell B-1. Figures (a) to (d) are CT images and figure (e) is a regular photograph of disassembled parts.

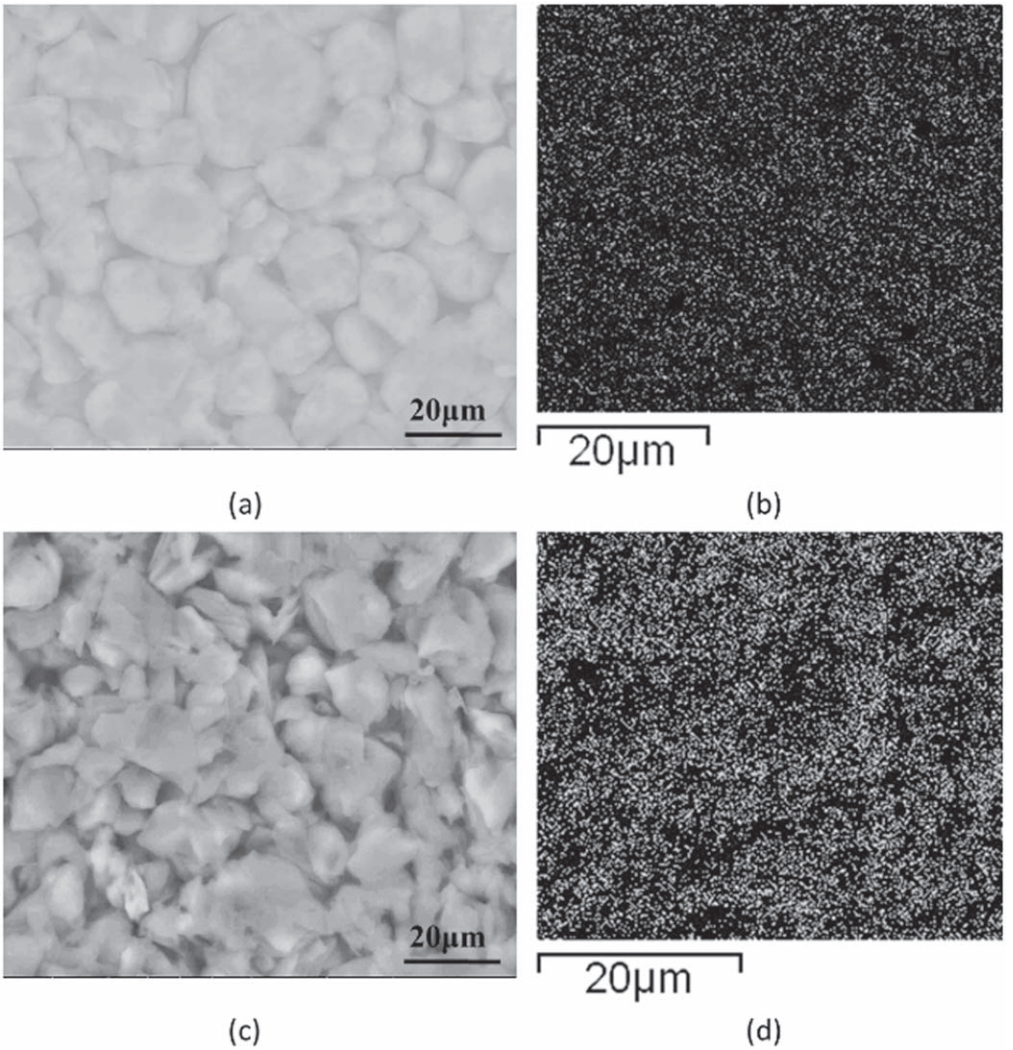


Figure 5. SEM image of the anode from (a) cell A-1 and (c) cell B-1; EDX mapping of carbon element for (b) cell A-1 and (d) cell B-1.

Table II. The anode elemental composition of cells A-1 and B-1.

Cell A-1	C	O	F	Cu	P	S	Total
Weight %	84.79	8.37	5.26	0.77	0.53	0.28	100
Atomic %	89.38	6.63	3.51	0.15	0.22	0.11	100
Cell B-1	C	O	F	Cu	P	S	Total
Weight %	80.97	11.90	5.64	0.80	0.57	0.12	100
Atomic %	86.24	9.52	3.80	0.16	0.23	0.05	100

Table III. The cathode elemental composition of cells A-1 and B-1.

Cell A-1	Co	O	C	Other Elements	Total
Weight %	41.26	29.75	20.64	8.35	100
Atomic %	14.85	39.42	36.42	9.31	100
Cell B-1	Co	O	C	Other Elements	Total
Weight %	45.13	28.18	17.34	9.35	100
Atomic %	17.20	39.56	32.43	10.81	100

Findings revealed that cathode from both cells A-1 and B-1 were combinations of active cathode material (lithium cobalt oxide; O, Co elements), binder (F element, PVDF), and carbon black (C element). The cell B-1 cathode contained cobalt element, which indicates the cathode material was lithium cobalt oxide instead of the NMC listed in the specification. During the elemental analysis, the area mapping (Fig. 6) and various point analyses (Fig. 7) were conducted on the sample from cell B-1. As shown in Fig. 7, particles with different sizes and morphologies were analyzed, the elemental spectrum from all the points are the same and spectrum 1 is shown as the example. Since the nickel and manganese were not found, the elemental analysis done on cell B-1 confirmed that the battery specification was not valid.

Electrode samples with around 1 $\times$ 1 cm^2 were cut from the disassembled battery and embedded in the epoxy resin matrix. After grinding, the cross-section of the electrode was revealed. The selected electrode samples from cell A-1 were observed under the ZEISS Axiovert microscope. The thickness was measured with the imaging software. In the case of cell A-1, the anode material coating thickness was around 65 μm; the anode current collector thickness was around 37 μm; the cathode material coating thickness was around 51 μm, and the cathode current collector thickness was

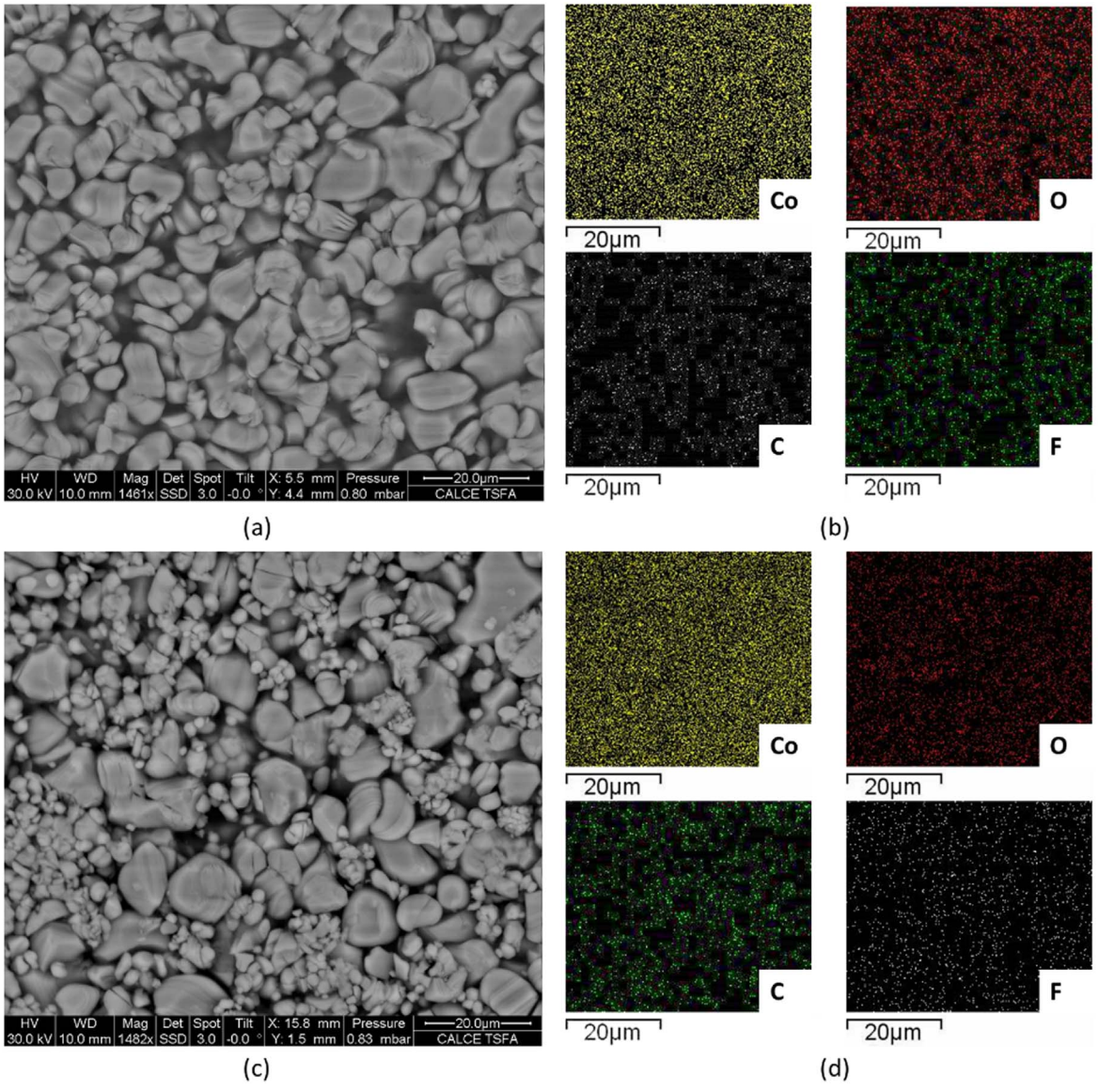


Figure 6. SEM image of the cathode from (a) cell A-1 and (c) cell B-1; EDX elemental mapping for (b) cell A-1 and (d) cell B-1.

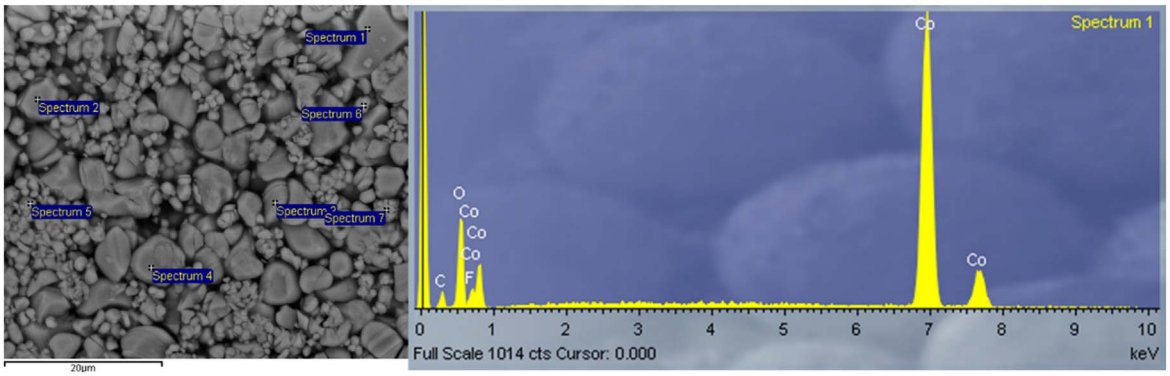


Figure 7. SEM image of the cathode from cell B-1 and the EDX spectrum from points 1 and 5.

around 26 μm. As for cell B-1, the anode material coating thickness was around 62 μm; the anode current collector thickness was around 26 μm; the cathode material coating thickness was around 62 μm, and the cathode current collector thickness was around 30 μm.

FTIR is used to obtain an infrared spectrum of absorption or emission of a solid, liquid, or gas. This work is used to analyze the characteristics of the material of the separators used in cells A-1 and B-1. Following this approach, after the cell disassembly, two separator pieces were cut from cells A-1 and B-1. The separator sample was cleaned to determine the separator composition. The characteristic absorbance bands for polyethylene (PE) were located at: 2919 cm^{-1}, 2851 cm^{-1}, 1473 cm^{-1}, and 720 cm^{-1} attributed to CH_2 asymmetric stretching, CH_2 symmetric stretching, bending deformation, and rocking deformation, respectively.[59] Cell A−1 (Fig. 8a) showed characteristic peaks at 2916, 2846, 1469, and 721 cm^{-1}. Cell B−1 (Fig. 8b) showed characteristic peaks at 2915, 2846, 1466, and 717 cm^{-1}. The material for both cell A-1 and cell B-1 separators was PE based on the characteristic absorbance bands. The manufacturer specification does not reveal the separator material, identification of separator material was expected by the device manufacturer.

Overall, the destructive tests showed deviations from listed specifications and faults caused by errors in manufacturing that may lead to safety risks. Electrochemical characterization or standards-based tests did not provide information necessary to identify these issues.

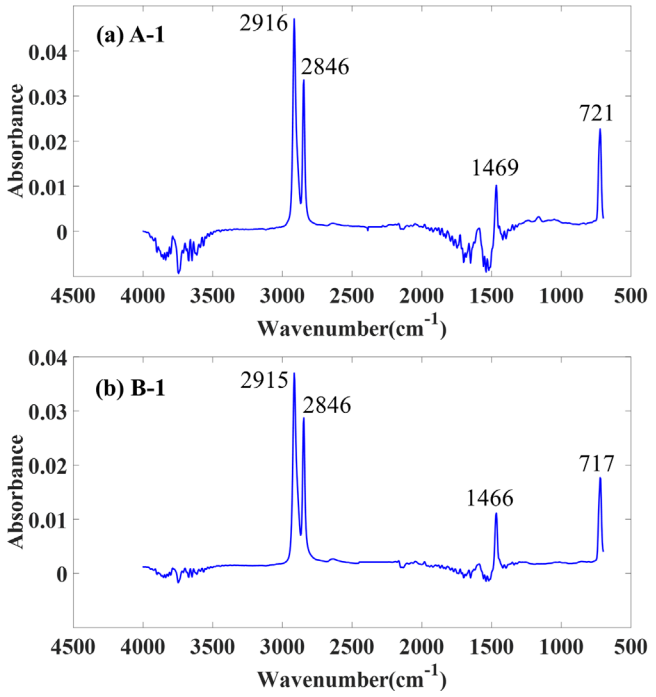


Figure 8. The IR spectrum from the cleaned separator sample from (a) cell A-1 and (b) cell B-1.

Conclusions

Alongside the lithium-ion battery mass-production, manufacturers conduct limited tests that focus on electrochemical performance. Potential failure precursors are overlooked. This paper addresses this challenge by including battery quality evaluation of assembly precision and material composition beyond electrochemical verification.

The results of the quality testing showed that the Type A battery has a stacked electrode configuration, and type B has a jelly-roll arrangement. The cell A manufacturer specification does not specify the cathode material type. Cathode material identification is also expected from the testing. The received battery specification indicated the cell B cathode was made of NMC. The electrochemical tests, including capacity and impedance measures, showed compliance with the manufacturers' specifications for both types of lithium-ion batteries. However, quality issues were identified in the battery assembly and material composition using a CT scan, disassembly, and material characterization for both batteries. For cell A-1, cathodes extended past anodes at the top and bottom of the roll. The anodes should cover the cathodes in order to make full use of active lithium content and prevent lithium dendrite growth. In addition, a CT scan showed deformities in the electrode that appeared near the corners. During the following disassembly, these electrode locations exhibited electrode coating peel off. The coating peel-off demonstrated that these locations experienced higher stress levels than the rest of the electrode. These locations could be the contact points between the electrode and the assembly line tools. For improving the battery quality, the assembly machine should apply force evenly on the electrodes. Cell B-1 showed gaps in the winding structure at the turning edges that can lead to nonuniform lithium-ion intercalation, potentially leading to dendrite growth and ultimately in short circuits. Another assembly-related defect was a folded electrode that can disrupt the current distribution and increase localized abrasion. Discrepancies existed for the cathode material. For cell B, the NMC material specified by the battery manufacturer turned out to be LCO.

From this analysis it can be concluded that lithium-ion battery quality evaluation should incorporate electrochemical performance tests and assessments of assembly precision and material composition. The electrochemical performance tests such as the internal impedance measurements, the cell initial capacity measurement, and the battery cycling test are widely adopted for battery testing. But the cycling test that takes months to perform is not compatible with mass production. Beyond the available testing methods, the non-destructive X-ray based imaging techniques, including X-ray photography and tomography (CT scan), have shown to be efficient in locating failure precursors within an assembled lithium-ion cell. The

X-ray photography scanner can be incorporated into the production process and developed into an online screening/binning step without causing a significant increase in the battery production cost. The scanner can be used to check whether the electrodes overlap or whether the electrodes align correctly. X-ray tomography (CT) and SEM/EDX are recommended for samples from each lot of batteries. The CT scan is used to examine the structure and the SEM/EDX analysis can determine whether the battery material matches the specification.

Acknowledgments

The authors thank the Center for Advanced Life Cycle Engineering (CALCE) and its over 150 funding companies and the Centre for Advances in Reliability and Safety (CAiRS) at Hong Kong for enabling research into advanced topics in reliability, safety, and sustainment.

ORCID

Lingxi Kong https://orcid.org/0000-0001-8387-1140
Mohammad Alipour https://orcid.org/0000-0002-7862-2729
Stanislav I. Stoliarov https://orcid.org/0000-0002-3429-9245

References

1. X. Zhu, Z. Wang, C. Wang, and L. Huang, *J. Electrochem. Soc.*, **165**, A3613 (2018).
2. R. M. Wittman, M. L. Perry, T. N. Lambert, B. R. Chalamala, and Y. Preger, *J. Electrochem. Soc.*, **167**, 090545 (2020).
3. N. Takami, K. Ise, Y. Harada, T. Iwasaki, T. Kishi, and K. Hoshina, *J. Power Sources*, **396**, 429 (2018).
4. M. Mathew, Q. H. Kong, J. McGrory, and M. Fowler, *J. Power Sources*, **349**, 94 (2017).
5. N. Atikah, A. H. A. Ghabid, W. Sutopo, A. Purwanto, and M. Nizam, "Technical feasibility for technology commercialization of battery lithium ion." *Proceedings of 2014 International Conference on Electrical Engineering and Computer Science, ICEECS 2014, 308–314* (2014).
6. C. W. Seitz, *IEEE Aerosp. Electron. Syst. Mag.*, **9**, 10 (1994).
7. Y. Sun, L. Kong, H. Abbas Khan, and M. G. Pecht, *IEEE Access*, **7**, 71131 (2019).
8. J. Schnell and G. Reinhart, *Procedia CIRP*, **57**, 568 (2016).
9. S. Santhanagopalan and R. E. White, *International Journal of Electrochemistry*, **2012**, 1 (2012).
10. C. W. Adams, C. S. Landes, D. G. Robertson, and M. W. Ferebee, "Continuous web inline testing apparatus, defect mapping system and related methods." *N/A*, WO2015061543 (2015).
11. U. Heider, R. Oesten, and M. Jungnitz, *J. Power Sources*, **81–82**, 119 (1999).
12. D. Mohanty, E. Hockaday, J. Li, D. K. Hensley, C. Daniel, and D. L. Wood, *J. Power Sources*, **312**, 70 (2016).
13. B. Kenney, K. Darcovich, D. D. MacNeil, and I. J. Davidson, *J. Power Sources*, **213**, 391 (2012).
14. Y. Wu, S. Saxena, Y. Xing, Y. Wang, C. Li, W. K. C. Yung, and M. Pecht, *Energies*, **11**, 925 (2018).
15. X. Feng, M. Fang, X. He, M. Ouyang, L. Lu, H. Wang, and M. Zhang, *J. Power Sources*, **255**, 294 (2014).
16. B. Wu et al., *J. Electrochem. Soc.*, **166**, A4141 (2020).
17. D. H. Doughty and E. P. Roth, *The Electrochemical Society Interface*, **21**, 37 (2012).
18. C. J. Mikolajczak, T. Hayes, V. M. Marcus, and M. Wu, "A Scientific Methodology for Investigation of a Lithium Ion Battery Failure." *in 2007 International Conference on Portable Information Devices, p. 1–6* (2007).
19. J. Li et al., *JOM*, **69**, 1484 (2017).
20. W. Choi, H. C. Shin, J. M. Kim, J. Y. Choi, and W. S. Yoon, *Journal of Electrochemical Science and Technology*, **11**, 1 (2020).
21. D. Mohanty, E. Hockaday, J. Li, D. K. Hensley, C. Daniel, and D. L. W. Iii, *J. Power Sources*, **312**, 70 (2016).
22. K. Rumpf, M. Naumann, and A. Jossen, *Journal of Energy Storage*, **14**, 224 (2017).
23. T. Günther, D. Schreiner, A. Metkar, C. Meyer, A. Kwade, and G. Reinhart, *Energy Technology*, **8** (2020).
24. G. Qian et al., *Cell Reports Physical Science*, **2**, 100554 (2021).
25. W. Huang, X. Feng, X. Han, W. Zhang, and F. Jiang, *Cell Reports Physical Science*, **2**, 100285 (2021).
26. Y. Zhang, C. Y. Wang, and X. Tang, *J. Power Sources*, **196**, 1513 (2011).
27. R. Zhang, B. Xia, B. Li, L. Cao, Y. Lai, W. Zheng, H. Wang, W. Wang, and M. Wang, *Energies*, **11**, 2408 (2018).
28. I. Bloom, A. N. Jansen, D. P. Abraham, J. Knuth, S. A. Jones, V. S. Battaglia, and G. L. Henriksen, *J. Power Sources*, **139**, 295 (2005).
29. N. Williard, B. Sood, M. Osterman, and M. Pecht, *J. Mater. Sci., Mater. Electron.*, **22**, 1616 (2011).
30. N. Zhang and H. Tang, *J. Power Sources*, **218**, 52 (2012).
31. A. Senyshyn, M. J. Mühlbauer, K. Nikolowski, T. Pirling, and H. Ehrenberg, *J. Power Sources*, **203**, 126 (2012).
32. A. Barai, K. Uddin, M. Dubarry, L. Somerville, A. McGordon, P. Jennings, and I. Bloom, *Prog. Energy Combust. Sci.*, **72**, 1 (2019).
33. S. M. Lambert, M. Armstrong, P. S. Attidekou, P. A. Christensen, J. D. Widmer, C. Wang, and K. Scott, *IEEE Trans. Ind. Electron.*, **64**, 4017 (2017).
34. A. Etiemble, N. Besnard, J. Adrien, P. Tran-Van, L. Gautier, B. Lestriez, and E. Maire, *J. Power Sources*, **298**, 285 (2015).
35. T. Waldmann, S. Gorse, T. Samtleben, G. Schneider, V. Knoblauch, and M. Wohlfahrt-Mehrens, *J. Electrochem. Soc.*, **161**, A1742 (2014).
36. M. J. Brand, S. F. Schuster, T. Bach, E. Fleder, M. Stelz, S. Gläser, J. Müller, G. Sextl, and A. Jossen, *J. Power Sources*, **288**, 62 (2015).
37. V. Yufit, P. Shearing, R. W. Hamilton, P. D. Lee, M. Wu, and N. P. Brandon, *Electrochem. Commun.*, **13**, 608 (2011).
38. S. Kim, Y. S. Lee, H. S. Lee, and H. L. Jin, *Materialwiss. Werkstofftech.*, **41**, 378 (2010).
39. IEEE, (2008), IEEE Std 1625-2008 10.1109/IEEESTD.2008.4657368.
40. T. Waldmann et al., *J. Electrochem. Soc.*, **163**, A2149 (2016).
41. V. Tarnopolskiy, J. Kalhoff, M. Nádherná, D. Bresser, L. Picard, F. Fabre, M. Rey, and S. Passerini, *J. Power Sources*, **236**, 39 (2013).
42. J. Vetter, P. Novák, M. R. Wagner, C. Veit, K. C. Möller, J. O. Besenhard, M. Winter, M. Wohlfahrt-Mehrens, C. Vogler, and A. Hammouche, *J. Power Sources*, **147**, 269 (2005).
43. J. H. Cheng, A. A. Assegie, C. J. Huang, M. H. Lin, A. M. Tripathi, C. C. Wang, M. T. Tang, Y. F. Song, W. N. Su, and B. J. Hwang, *J. Phys. Chem. C*, **121**, 7761 (2017).
44. J. M. Tarascon, *J. Electrochem. Soc.*, **141**, 1421 (1994).
45. G. Gachot, P. Ribière, D. Mathiron, S. Grugeon, M. Armand, J. B. Leriche, S. Pilard, and S. Laruelle, *Anal. Chem.*, **83**, 478 (2011).
46. M. N. Richard, *J. Electrochem. Soc.*, **146**, 2078 (1999).
47. I. Bardenhagen, O. Yezerska, M. Augustin, D. Fenske, A. Wittstock, and M. Bäumer, *J. Power Sources*, **278**, 255 (2015).
48. J. Cannarella and C. B. Arnold, *J. Power Sources*, **226**, 149 (2013).
49. N. Shpigel, S. Sigalov, M. D. Levi, T. Mathis, L. Daikhin, A. Janes, E. Lust, Y. Gogotsi, and D. Aurbach, *Joule*, **2**, 988 (2018).
50. N. Schulz, R. Hausbrand, C. Wittich, L. Dimesso, and W. Jaegermann, *J. Electrochem. Soc.*, **165**, A833 (2018).
51. B. Stiaszny, J. C. Ziegler, E. E. Krauß, M. Zhang, J. P. Schmidt, and E. Ivers-Tiffée, *J. Power Sources*, **258**, 61 (2014).
52. R. J. Brodd and C. Helou, *J. Power Sources*, **231**, 293 (2013).
53. J. Schmitt, A. Raatz, F. Dietrich, K. Dröder, and J. Hesselbach, *CIRP Annals - Manufacturing Technology*, **63**, 9 (2014).
54. J. Kurfer, M. Westermeier, C. Tammer, and G. Reinhart, *CIRP Annals - Manufacturing Technology*, **61**, 1 (2012).
55. IEEE, (2021), IEEE Std 1725-2021 10.1109/IEEESTD.2021.9514813.
56. C. Brissot, M. Rosso, J. N. Chazalviel, P. Baudry, and S. Lascaud, *Electrochim. Acta*, **43**, 1569 (1998).
57. C. R. Birkl, M. R. Roberts, E. McTurk, P. G. Bruce, and D. A. Howey, *J. Power Sources*, **341**, 373 (2017).
58. F. Grimsmann, T. Gerbert, F. Brauchle, A. Gruhle, J. Parisi, and M. Knipper, *Journal of Energy Storage*, **15**, 17 (2018).
59. J. v. Gulmine, P. R. Janissek, H. M. Heise, and L. Akcelrud, *Polym. Test.*, **21**, 557 (2002).